

**Resonant coherent excitation of  $N^{6+}$  and  $Mg^{11+}$  in planar channeling: anisotropies in ionization probabilities and X-ray emission**

S. Datz, P. F. Dittner, H. F. Krause, C. R. Vane, and O. H. Crawford

*Physics Division, P. O. Box 2008, Oak Ridge National Laboratory  
Oak Ridge, Tennessee 37831-6377 USA*

J. S. Forster, G. S. Ball, W. G. Davies, and J. S. Geiger

*AECL Research  
Chalk River Laboratories  
Chalk River, Canada*

The thrust of the conference in which this paper is presented is toward inelastic interactions of ions with surfaces. The work described in this paper deals with inelastic interactions of ions in planar channeling inside the crystal. We are, however, not too far off the mark because the planar channeling potential is made up from the sum of two (sheet) "surface potentials. The difference, if you will, is similar to that between an ordinary sandwich and an open faced one (smørebrod), and in the future these techniques may well be applied to the single surface.

In earlier work on resonant coherent excitation (RCE) of channeled ions, it was shown that for H-like ions ( $Z = 4 - 9$ ) moving in axial crystal channels in the velocity range  $6 v_0 \leq v_i \leq 12 v_0$ , collisional lifetimes are sufficiently long to give well-defined  $n=1$  and  $n=2$  states. It was also shown that the effect of the spatially (time) coherent field caused by correlated collisions with atoms arranged in crystal rows can give rise to resonant excitation of the penetrating ion [1,2]. Thus, an ion moving at velocity  $v_i$  past a row of atoms with interatomic spacing  $d$  experiences periodic perturbation at frequencies  $\nu = K(v_i/d)$ ,  $K = 1, 2, 3, \dots$ . The ion can be resonantly excited when a frequency  $\Delta E_{ij}/h$  is attained, where  $\Delta E_{ij}$  is the energy difference between states  $i$  and  $j$  of the moving ion. We showed that the energy levels of the penetrating ion differed measurably from the vacuum states. These differences reflected the influence of the static crystal field which removed the degeneracy of the  $2p_x$ ,  $2p_y$ , and  $2p_z$  orbitals, and of the influence of wake field which acted to Stark mix the  $2s$  and  $2p_z$  states.

**MASTER**

"The submitted manuscript has been authored by a contractor of the U.S. Government under contract No. DE-AC05-84OR21400. Accordingly, the U.S. Government retains a nonexclusive, royalty-free license to publish or reproduce the published form of this contribution, or allow others to do so, for U.S. Government purposes."

## **DISCLAIMER**

**Portions of this document may be illegible in electronic image products. Images are produced from the best available original document.**

It was then shown that, while in axial channeling, the excitation frequencies are determined by the fixed spacing along rows in a given lattice direction, in planar channeling, the frequencies are vector sums of components in the  $hk\ell$  directions [3]. Hence, at a given velocity (see Fig. 1), a continuously tunable range of resonant frequencies is available depending on the angle in the plane low index axial directions. In both cases, (axial and planar), the resonances were previously observed by varying the ion beam energy for a fixed crystal orientation.

An example of the resonances that can be attained is shown in Fig. 2 for  $N^{6+}$  in the (100) planar channel of Au, where a plot of the velocities and angles required to achieve RCE for  $n=1 \rightarrow n=2$  is shown. The condition for resonance in the (100) plane of an FCC lattice is given by

$$E_r(\text{MeV/amu}) = 3.03 \times \frac{2}{(\gamma+1)} \times \left[ \frac{\Delta E_{ij}(\text{keV}) \times a(\text{\AA})}{\ell \cos\theta + k \sin\theta} \right]^2 \quad (1)$$

where  $E_r$  is the resonant ion energy,  $\gamma$  is the relativistic factor  $(\sqrt{1-\beta^2})^{-1}$ ,  $a$  is the lattice constant and  $\ell$  and  $k$  are field components. The resonances are denoted by  $(\ell, k)$  in the diagram.

For the low-Z (4-9) hydrogenic ions used, the resonances were demonstrated by observing the increase in the fraction of totally stripped ions which occurred as the ion passed through the crystal channel as a function of  $v_i$ . The reason for this increase is the increase in the ionization cross section (factor  $\sim 10$ ) which occurs when the ion is pumped up from  $n=1 \rightarrow n=2$ . For the ions in question, there is a reasonable chance ( $\sim 50\%$ ) of the ion in its 1s state, passing through the electrons in the channel without electron loss, however, in the  $n=2$  state, the probability of emergence from even these very thin (1000 - 5000  $\text{\AA}$ ) crystals is vanishingly small.

This is not true for higher-Z ions at higher velocities. Here the ionization cross section of even the  $n=2$  state may be small enough to allow the ion to escape from the crystal intact where it is then free to relax via radiative decay. This was demonstrated in a later paper [4] using  $Mg^{11+}$  ions and observing RCE in the 7th harmonic in the  $\langle 111 \rangle$  axial channel in Au at resonant velocities of  $\sim 16 v_0$  ( $\sim 160$  MeV). Here the resonance could be observed by either an increase in

Mg<sup>12+</sup> population or by an increase in Mg<sup>11+</sup> Ly<sub>α</sub> X radiation from those ions which escaped the crystal in the n=2 state. Differences in the relative population of the 2p<sub>z</sub> and 2p<sub>x</sub> states were noted between the radiative and ionization channels implying differences in the electron bombardment ionization cross sections for these two orbitals.

This result led to a curious conclusion: namely, that the specific m state population created by RCE retained its identity long enough to participate in an ionizing collision, i.e., the alignment was not destroyed by electron collisions prior to the ionizing collision. This result could be due to the creation of these states in different parts of the channel, e.g., the 2p<sub>x</sub> state might be created closer to the atomic strings than the 2p<sub>z</sub> and result in a higher probability for ionization of 2p<sub>x</sub> states. Since trajectories in axial channeling are extremely complex, we sought to carry out the experiments in planar channels where the trajectories are considerably simpler to follow. In addition, we would like to work with low harmonics where the transition strength is large and to use ions which can give X rays which are measurable with a SiLi detector (~>1 keV), i.e., we must use high energy beams to achieve low harmonics.

These requirements lead to a dilemma if we are to carry out these experiments as we have in the past, i.e., to use H-like ions and vary the ion beam energy in small steps. To achieve the high energies in question requires the use of a cyclotron or linac where small variations in ion beam energy by varying machine conditions are not achieved on a short time scale. The usual method is to accelerate to a higher energy and then "degrade" the energy by passing it through an absorber and selecting the final energy via magnetic deflection. Unfortunately, at the desired high energies, almost all the ions emerging from the degrader would be totally stripped with very little H-like component remaining. This led us to examine the possibility of studying these resonances using a beam of fixed velocity and varying instead the distance *d* between perturbing centers, i.e., using planar channeling with a fixed ion beam energy and varying angle (see Eq. (1)).

The lowest achievable planar harmonic is the (2,0) which lies in energy above the 2nd harmonic in the <100> axis (see Fig. 2). We investigated the feasibility of the angle variation

technique  $N^{6+}$  ions from the ORNL EN Tandem Van de Graaff at energy of 3.25 MeV/amu where excitation to  $n=2$  is tantamount to ionization. To investigate the region where escape with subsequent radiation contributes, we employed  $Mg^{11+}$  ions at an energy of 25 MeV/amu using the Chalk River CSCC Tandem Cyclotron Facility.

### Experimental Arrangement

The general experimental arrangement has been described previously [4]. For the nitrogen experiment, a beam of  $N^{6+}$  ions at an energy of 3.25 MeV/amu was supplied by the ORNL EN Tandem accelerator. After suitable collimation, it was passed through an Au crystal (1800 Å thick). The Au crystal was epitaxially grown on rock salt with the surface parallel to a (100) plane, mounted in a 3-axis goniometer and oriented so that it could be rotated about a  $\langle 100 \rangle$  axis toward a  $\langle 110 \rangle$  axis, i.e., in the (100) plane. The emergent charge-state distribution was analyzed by electrostatic deflection followed by a solid-state position-sensitive detector. Charge states 5, 6, and 7 were simultaneously detected.

In the case of  $Mg^{11+}$  (see Fig. 3), the beam was supplied at an energy of 25 MeV/amu by the CSCC Tandem Cyclotron Facility at Chalk River, Canada, and passed through an Ni crystal 4000 Å thick which was epitaxially grown with the surface parallel to a (100) plane. As above, the crystal could be rotated about a  $\langle 100 \rangle$  axis in the (100) plane. The beam was charge state analyzed by a Q3D magnetic analyzer in which charges 11+ and 12+ were registered. At the energy in question, almost no 10+ fraction is visible. Two Si(Li) X-ray detectors aimed at 90° and 45° recorded the emission of  $Mg^{11+}$   $Ly\alpha$  ( $n=2 \rightarrow 1$ ) X rays.

### Results and Discussion

We expect that different substates in the  $n=2$  manifold will be non-degenerate and will occur at different exciting frequencies. Further, these energy levels may be a function of distance from the center of the channel. Calculations of these energy levels have been carried out and the results for, e.g.,  $N^{6+}$  at 3.25 MeV/amu in (100) Au are shown in Fig. 4. The vertical scale denotes the energy difference between these states and the level they would have in vacuum.

The horizontal axis corresponds to the distance from the center of the channel. The energy shifts of the excited states and the transition strengths were calculated from a time-dependent effective-Hamiltonian theory described previously [5]. Inputs to the calculation included electron scattering factors [6], and the plasmon energies of Ni and Au (assumed to be 20.7 eV and 25.8 eV, respectively). The wave functions for these states also depend on the distance between the ion and the atomic planes. These are represented by the cartoons in Fig. 5. At the center of the channel, the  $2p_z$  state is Stark mixed with the  $2s$  to form two states: one with a forward pointing lobe and the other with a rear pointing lobe. Moving away from the channel center, the transverse field dominates the Stark mixing and the  $2s$  mixes with  $2p_x$ , the  $2p_z$  becomes a single symmetric state. The  $2p_x$  state, which at channel center is a symmetric state, mixes with  $2s$  to form two states; one  $2p_x 2s(c)$  with the largest lobe pointing toward the center and the other  $2p_x 2s(w)$  with its largest lobe pointing toward the channel wall. Since there is no gradient in its direction, the  $2p_y$  state is symmetric at all distances.

Figure 6 shows the calculated transition strength for each of these states as a function of distance from the channel center. Extending furthest into the potential gradient, the  $2p_x 2s(w)$  state has the highest value. The  $2p_y$  has by far the lowest. The main point here, however, is that the transition strength is least at the channel center and increases sharply as the "wall" is approached. Returning to Fig. 4, we see that the energy of the  $2p_z$  state is relatively constant with distance and should therefore appear as a sharp line at an energy just  $\sim 2-5$  eV below the vacuum level. The  $2p_x 2s(w)$  state, on the other hand, should appear as a broad feature extending to  $\sim 30$  eV below the vacuum level. The  $2p_x 2s(c)$  should appear as a narrower feature on the high energy side extending up to  $\sim 8$  eV above vacuum level. The  $2p_y$ , although relatively flat, has a very small transition strength at all distances and can be neglected.

The question arises as to where in the channel the excitation takes place? Motion of ions in planar channels have been extensively studied [7] and the answer is relatively simple. The ions oscillate in an almost harmonic potential of the form  $V(x) \sim A \cosh (bx)$  as shown in Fig. 7. Because of the relative flatness of the  $2p_z$  state energy with position, it will, at the proper angle,

receive continuous excitation almost everywhere along its path; the greatest will occur at its maximum amplitude. The situation for, e.g., the  $2p_x 2s(w)$  is quite different. Its energy level is changing continuously with position in the channel. In order to build up phase coherence at a given velocity, it must move in a region where the eigenstate is relatively constant. This it does only when it is at its maximum amplitude. It is here also that the transition strength is a maximum. Therefore, when we observe a resonance at a given angle, we can associate with it a given transition energy and a given position in the channel.

The observed charge state fractions of  $N^{6+}$  exiting the Au crystal are shown in Fig. 8. Along the top, we plot the angle in the (100) plane from the  $\langle 100 \rangle$  axis. Along the bottom, we plot the energy required for a (2,0) planar resonance as calculated from Eq. (1). The main (2,0) structure is contained in the region of 5 to 25°. The  $\Delta E_{1s \rightarrow 2p}$  in vacuum for the  $N^{6+}$  ion is at 500 eV. Three main features are contained in the spectrum, two peaks centered on either side of the vacuum level energy, and a broad feature extending out to almost 30 eV below the vacuum level. The feature on the high energy side extends to  $\sim 6$  eV. Using Fig. 3, these features can be identified below.

The sharp feature centered at -3 eV is due to the  $2p_z$  resonance. Its sharpness arises from the relative insensitivity of  $\Delta E_{ij}$  to position in the channel. If one includes the fact that the transition strength increases with increasing distance (Fig. 4), we expect a downshift of the  $2p_z$  peak of -3 to 5 eV. The shoulder on the high energy side is identified with the  $2p_x 2s(c)$  resonance which we expect to extend up to  $\sim 5-8$  eV. The very broad feature extending down to  $\sim 470$  eV is the  $2p_x 2s(w)$  resonance. (Note: The small features at 482 eV and 479 eV are due a higher order resonance (3,1) which overlays the (2,0) extend (Fig. 2). The feature at  $\sim 509$  eV is a portion of the (2,2) resonance which lies very close to the axis.)

The corresponding information for  $Mg^{11+}$  at 25 MeV/amu in (100) Ni is shown in Figs. 9, 10 and 11. Nickel was chosen for this experiment rather than gold because the smaller lattice constant  $d = 3.524 \text{ \AA}$  as against  $d = 4.078 \text{ \AA}$  in Au allowed us to reach the desired (2,0) resonance with the 25 MeV/amu beam available.

Because of the higher velocity and the higher  $Z$  of  $\text{Mg}^{11+}$  as compared with  $\text{N}^{6+}$ , the displacements from  $\Delta E_{1s \rightarrow 2p}$  are smaller. (Fig. 9 vis a vis Fig. 4). The transition strengths are of the same order of magnitude. However, in contrast to  $\text{N}^{6+}$  in Au (Fig. 6), the transition strength for  $2p_z$  lies slightly below that for  $2p_x 2s(c)$ , see Fig. 10. Similar identifications of the features can be made. The vacuum level  $\Delta E_{1s \rightarrow 2p}$  for  $\text{Mg}^{11+}$  is at 1472 eV. The  $2p_z$  peak is virtually coincident with this value. The  $2p_x 2s(c)$  forms a shoulder on the high energy side extending up to  $\sim 10$  eV above  $2p_z$  and the  $2p_x 2s(w)$  forms a bulge on the low energy side extending down to  $\sim 20$  eV below the vacuum resonance level.

Thus far, we have looked for effects due to  $n=1 \rightarrow n=2$  excitation followed by ionization. We now look for effects for ions which have been excited and survive to exit the crystal and then relax radiatively by X-ray emission. The results of the X-ray measurements on  $\text{Mg}^{11+}$  are shown in Fig. 12 and compared with the ionization measurements. The first obvious observation is that the X rays attributable to states excited to the  $2s 2p_x(w)$  are strongly suppressed when compared to emission from ions excited to the  $2p_z$  state. The relative probability of excitation to  $2s 2p_x(w)$  and  $2p_z$  is almost independent of position (amplitude), see Fig. 10. Hence, the difference in ionization probability is attributable to the shape of the wave function. This is not an unexpected result since the bulk of the square of the wave function for the  $2p_x 2s(w)$  state lies perpendicular to the direction of the bombarding electron flux and extends into regions of higher electron density near the planes of atomic cores. Although the shapes of the wave functions for these two states (i.e.,  $2p_z$  and  $2p_x 2s(w)$ ) vary with position (Fig. 5), their identities are reasonably clear. A  $2p_z$  mixed with  $2s$  on axis becomes almost pure  $2p_z$  far off axis. The  $2p_x 2s(w)$  state is a pure  $2p_x$  on axis but mixes with  $2s$  as it moves away from the axis. The case for the  $2p_x 2s(c)$  state is not as clear. The wave function for this state changes character drastically as it moves through its oscillation in the channel. In its on-axis manifestation, it is a  $2s$  mixed with  $2p_z$ . In its extreme form far off-axis, it is a  $2s$  mixed with a  $2p_x$ . In between, it has  $s$ ,  $p_z$  and  $p_x$  character.

Moving at 25 MeV/amu ( $\beta=0.23$ ), the velocity of the Mg ions is  $6.8 \times 10^9$  cm sec $^{-1}$  in which case they spend  $0.6 \times 10^{-14}$  sec in the 4000 Å crystal. The lifetime of  $2p \rightarrow 1s$  transition in

$\text{Mg}^{11+}$  is  $7.6 \times 10^{-14}$  sec so that almost all the observed radiation takes place outside the crystal. When the excited ions emerge from the crystal into vacuum, they must assume discrete states,  $2p_x$ ,  $2p_z$  or  $2s$ . The fraction appearing in a given state will depend on the vertical displacement in the planar channel at the exit point. The radiative lifetime for the  $2s \rightarrow 1s$  transition in  $\text{Mg}^{11+}$  is  $3 \times 10^{-7}$  sec so that very little  $2s$  radiation will occur within the field of view of the Si(Li) detectors. The radiation pattern of the  $2p_x$  state is orthogonal to the  $x$  direction. It should be isotropic in the  $y$ - $z$  plane and no differences in intensity should be observed between the  $90^\circ$  and  $45^\circ$  detectors (after correction for lab-frame to projectile-frame solid angles). The radiation pattern for the  $2p_z$  state is orthogonal to the  $z$  direction, isotropic in the  $x$ - $y$  plane and should display an increased intensity of  $90^\circ$  detector compared with the  $45^\circ$ . Such an effect is visible in Fig. 12. Here again the  $2p_x 2s(c)$  state is more complex. Although the state lies perpendicular to the electron flux, it always extends into regions of lower electron density. Its state depends on vertical displacement at the exit point. From the X-ray yield, it is evident that there is a chance for escape from the crystal without ionization and that it shows evidence for alignment.

In conclusion, there is strong evidence that once a given ionic state is excited, a large fraction of the ions remain in that state and are either ionized or radiate from that state. The result is counter to the expectation that electron-ion collisions in the channel would have a large enough cross section to destroy the alignment before either of these two events could take place. At this point, the reasons for the observed retention of anisotropy are open to conjecture.

The authors wish to express their appreciation to J. Chevallier of the Institute of Physics and Astronomy at Aarhus University, Denmark for his preparation of the crystals used in these experiments. The research by the Oak Ridge National Laboratory group is sponsored by the U.S. Department of Energy, Office of Basic Energy Sciences, Division of Chemical Sciences, under Contract No. DE-AC05-84OR21400 with Martin Marietta Energy Systems, Inc.

**References**

- [1] S. Datz, C. D. Moak, O. H. Crawford, H. F. Krause, P. F. Dittner, J. Gomez del Campo, J. A. Biggerstaff, P. D. Miller, P. Hvelplund, and H. Knudsen, *Phys. Rev. Lett.* **40**, 843 (1978).
- [2] C. D. Moak, S. Datz, O. H. Crawford, H. F. Krause, P. F. Dittner, J. Gomez del Campo, J. A. Biggerstaff, P. D. Miller, P. Hvelplund, and H. Knudsen, *Phys. Rev.* **A19**, 977 (1979).
- [3] S. Datz, C. D. Moak, O. H. Crawford, H. F. Krause, P. D. Miller, P. F. Dittner, J. Gomez del Campo, J. A. Biggerstaff, H. Knudsen, and P. Hvelplund, *Nucl. Instrum. Meth.* **170**, 18 (1980).
- [4] S. Datz, P. F. Dittner, J. Gomez del Campo, K. Kimura, H. F. Krause, C. R. Vane, Y. Iwata, K. Komaki, Y. Yamazaki, F. Fujimoto, and Y. Honda, *Rad. Effects and Defects in Solids* **117**, 73 (1991).
- [5] O. H. Crawford and R. H. Ritchie, *Phys. Rev.* **A20**, 1848 (1979).
- [6] P. A. Doyle and P. S. Turner, *Acta Cryst.* **A24**, 390 (1968). I used their Eq. (4), with parameters from Table 4(a).
- [7] See, e.g., S. Datz and C. D. Moak, "Heavy Ion Channeling" in Heavy Ion Science, Volume 6, D. A. Bromley, ed., Plenum Press (1983) pp. 169-240.

**DISCLAIMER**

This report was prepared as an account of work sponsored by an agency of the United States Government. Neither the United States Government nor any agency thereof, nor any of their employees, makes any warranty, express or implied, or assumes any legal liability or responsibility for the accuracy, completeness, or usefulness of any information, apparatus, product, or process disclosed, or represents that its use would not infringe privately owned rights. Reference herein to any specific commercial product, process, or service by trade name, trademark, manufacturer, or otherwise does not necessarily constitute or imply its endorsement, recommendation, or favoring by the United States Government or any agency thereof. The views and opinions of authors expressed herein do not necessarily state or reflect those of the United States Government or any agency thereof.

---

### Figure Captions

- Fig. 1 Coordinate system for planar channeling in the (100) plane of an FCC crystal.
- Fig. 2. Positions in energy and angle in the (100) plane for RCE resonances in the  $N^{6+} + Au(100)$  system. The horizontal dashed line indicates the region of angle scan of 3.25 MeV/amu  $N^{6+}$  discussed in this paper.
- Fig. 3. Schematic for the RCE experiment using the 25 MeV/amu  $Mg^{11+}$  beam at the Chalk River TASCC. The experiment on  $N^{6+}$  at ORNL did not use Si(Li) detectors.
- Fig. 4. Energy shifts of the various  $n=2$  substates from vacuum level  $\Delta E^\circ$ , as a function of distance from the planar channel midplane. The calculation here is for 3.25 MeV/amu  $N^{6+}$  in a (100) channel of Au  $10^\circ$  from  $\langle 100 \rangle$  axis. ----  $2p_x 2s(c)$ , —  $2p_y$ , ---  $2p_z$  — — —  $2p_x 2s(w)$ .
- Fig. 5. Wave function shapes for the substates as a function of distance from the channel midplane.
- Fig. 6. Transition strengths for the substates calculated here for 3.25 MeV/amu  $N^{6+}$  in (100) Au  $10^\circ$  from  $\langle 100 \rangle$  axis. ----  $2p_x 2s(c)$ , —  $2p_y$ , ---  $2p_z$  — — —  $2p_x 2s(w)$ .
- Fig. 7. Trajectories of ions entering a planar channel as a function of entrance point.
- Fig. 8. Surviving charge fraction of  $N^{6+}$  (3.25 MeV/amu) in (100) Au as a function of tilt angle from  $\langle 100 \rangle$  (top scale). This angle can be related to transition energy through Eq. (1). Aside from the overall structure due to the (2,0) resonance, a fraction of the (2,2) resonance can be seen near  $0^\circ$  and features due to higher order (3,1) resonances can be seen near  $20^\circ$ , see Fig. 2. The structure ranging from  $\sim 475$  to 500 eV is attributable to the  $2p_x 2s(w)$  state, the peak at 502 eV is due to the  $2p_z$  state, and the shoulder going up to  $\sim 506$  eV is due to the  $2p_x 2s(c)$  state.
- Fig. 9. Energy shifts of the various  $n=2$  substates from vacuum level  $\Delta E^\circ$ , as a function of distance from the planar channel midplane. The calculation here is for 25 MeV/amu  $Mg^{11+}$  in a (100) channel of Ni  $10^\circ$  from  $\langle 100 \rangle$  axis. ----  $2p_x 2s(c)$  state —  $2p_y$ , ---  $2p_z$  — — —  $2p_x 2s(w)$ .

**Figure Captions (contd)**

Fig. 10. Transition strengths for the substates calculated here for 25 MeV/amu  $Mg^{11+}$  in (100) Ni  $10^\circ$  from  $\langle 100 \rangle$  axis. ----  $2p_x 2s(c)$  —  $2p_y$ , ---  $2p_z$  — — — —  $2p_x 2s(w)$ .

Fig. 11. Surviving charge fraction of  $Mg^{11+}$  (25 MeV/amu) in (100) Ni as a function of tilt angle from  $\langle 100 \rangle$  (top scale). The angle can be related to transition energy through Eq. (1). The region from 1440 eV to 1470 eV can be attributed to the  $2p_x 2s(w)$  state, the peak at 1472 eV is due to the  $2p_z$ , and the shoulder extending up to  $\sim 1485$  eV is due to the  $2p_x 2s(c)$  state.

Fig. 12. X-ray yields in detectors placed at angles of  $45^\circ$  and  $90^\circ$  to the beam as a function of transition energy (tilt angle) as compared with charge state fraction (i.e., Fig. 11).

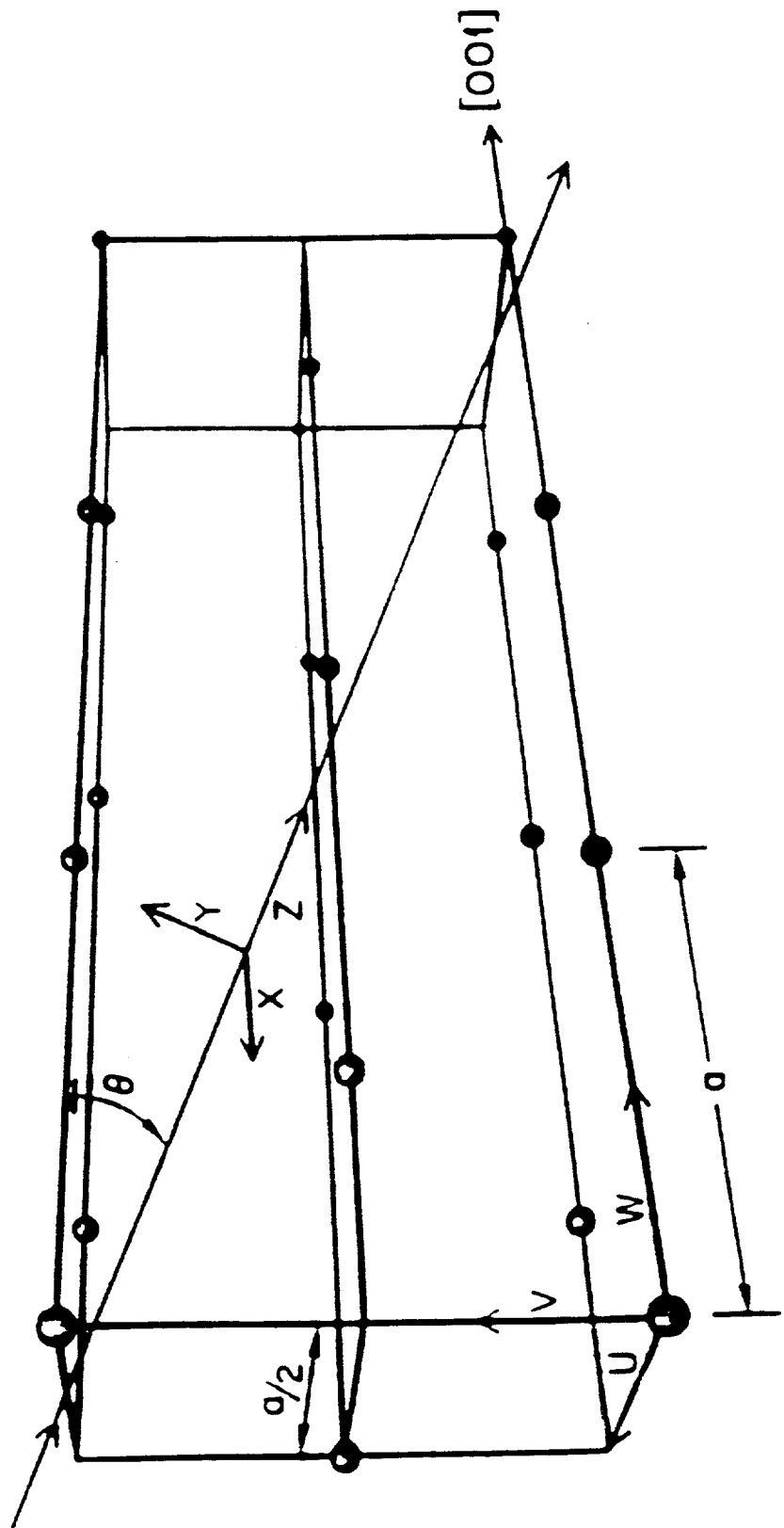


Figure 1

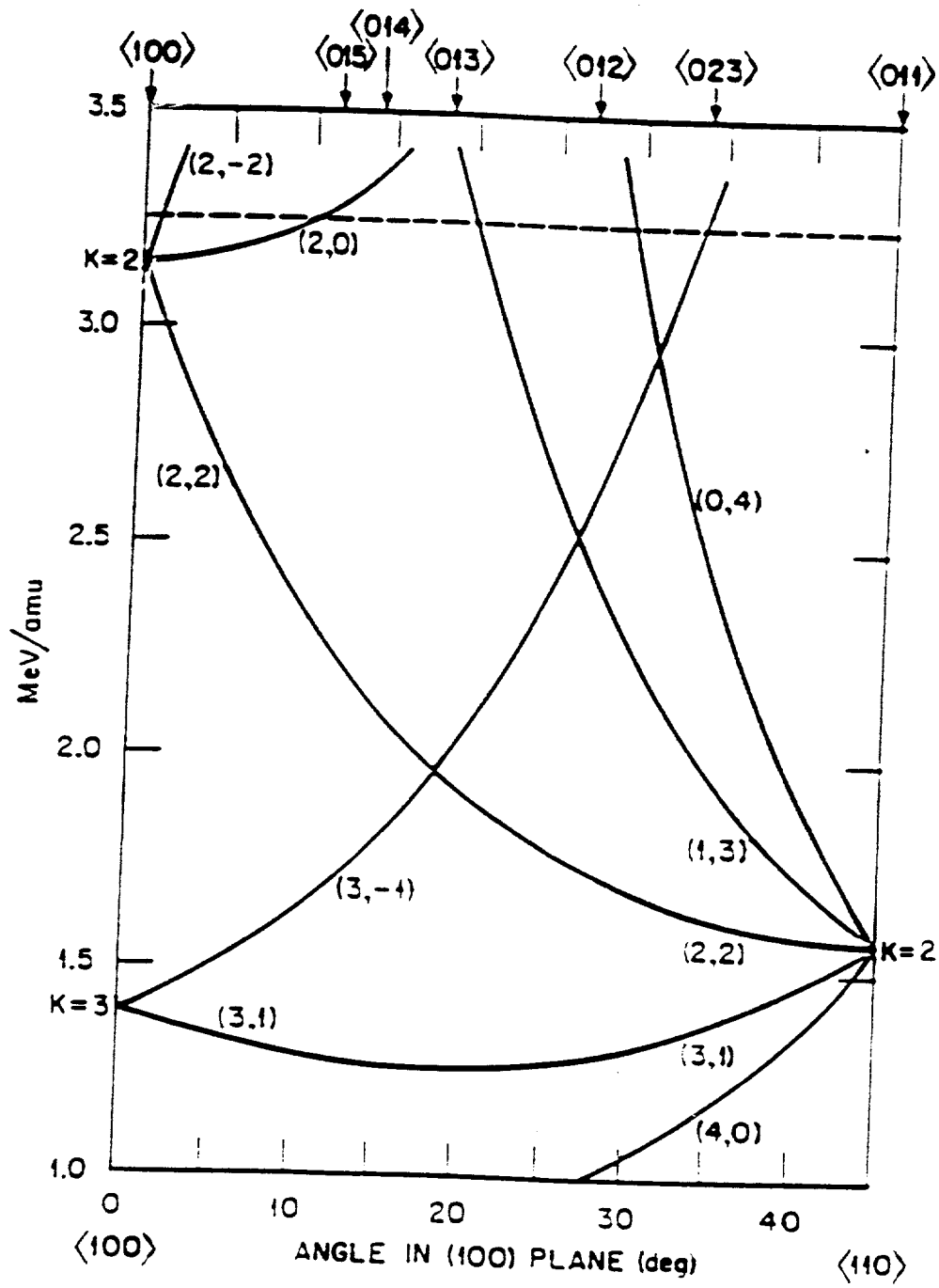


Figure 2

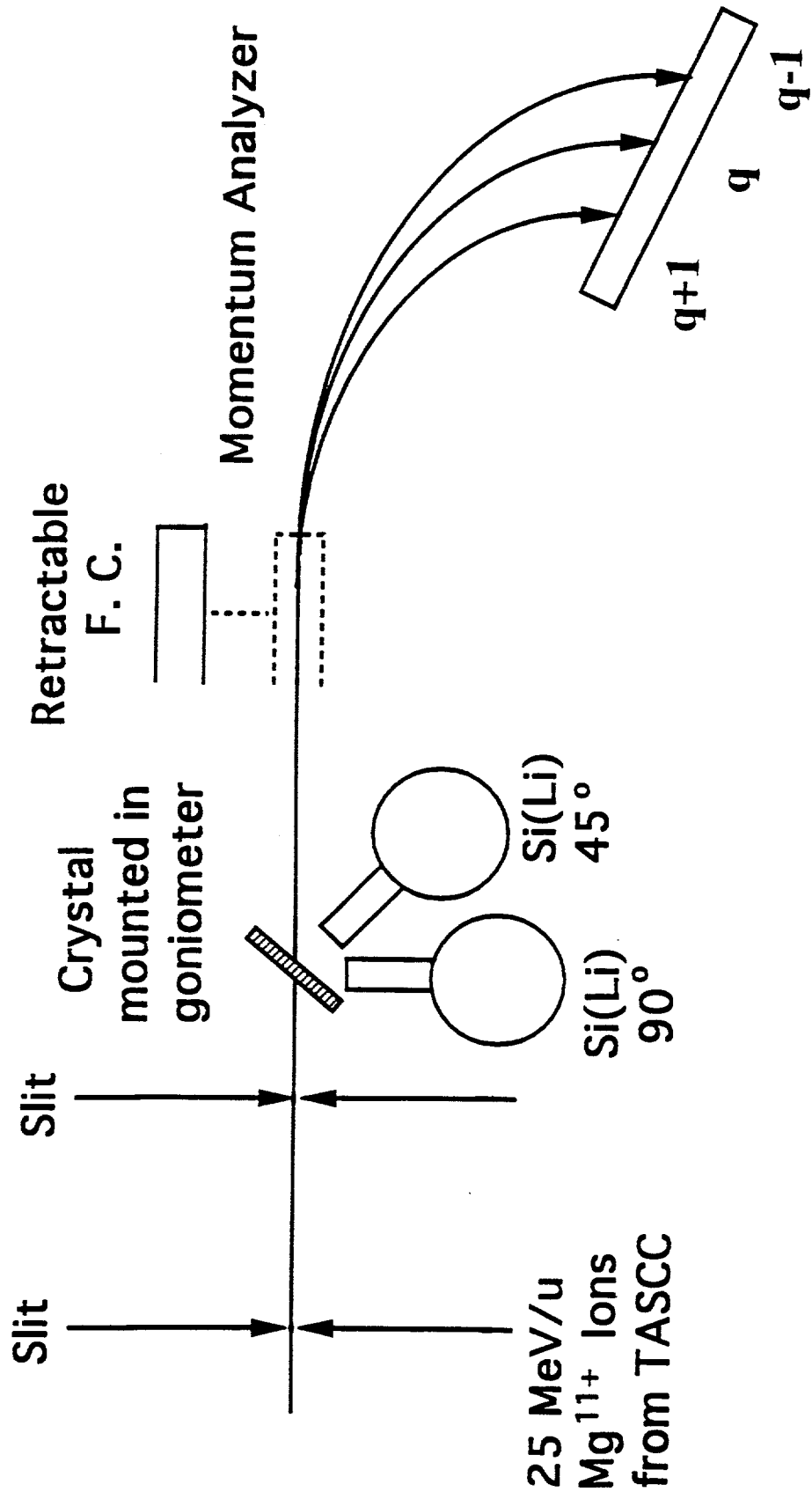


Figure 3

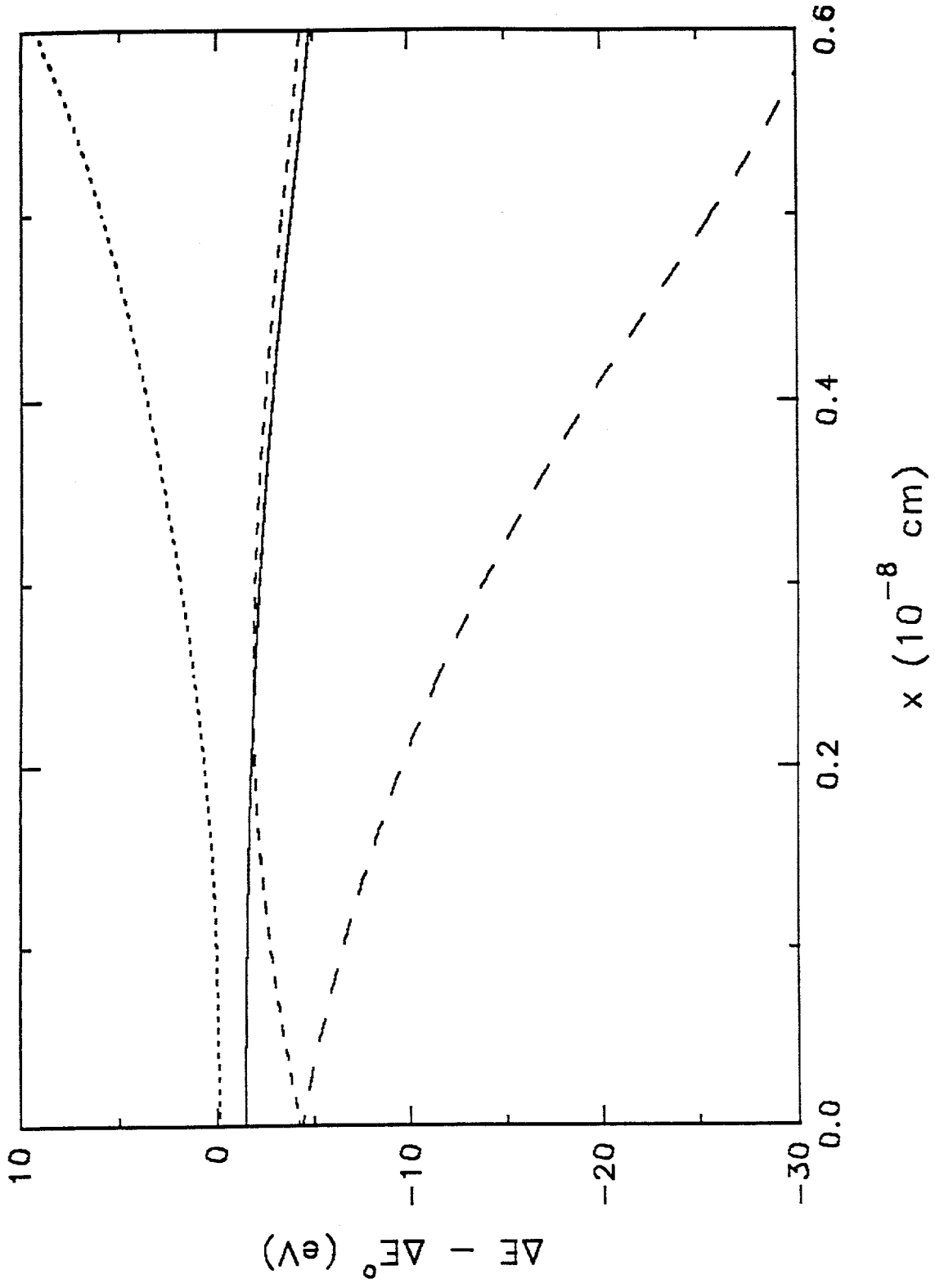


Figure 4

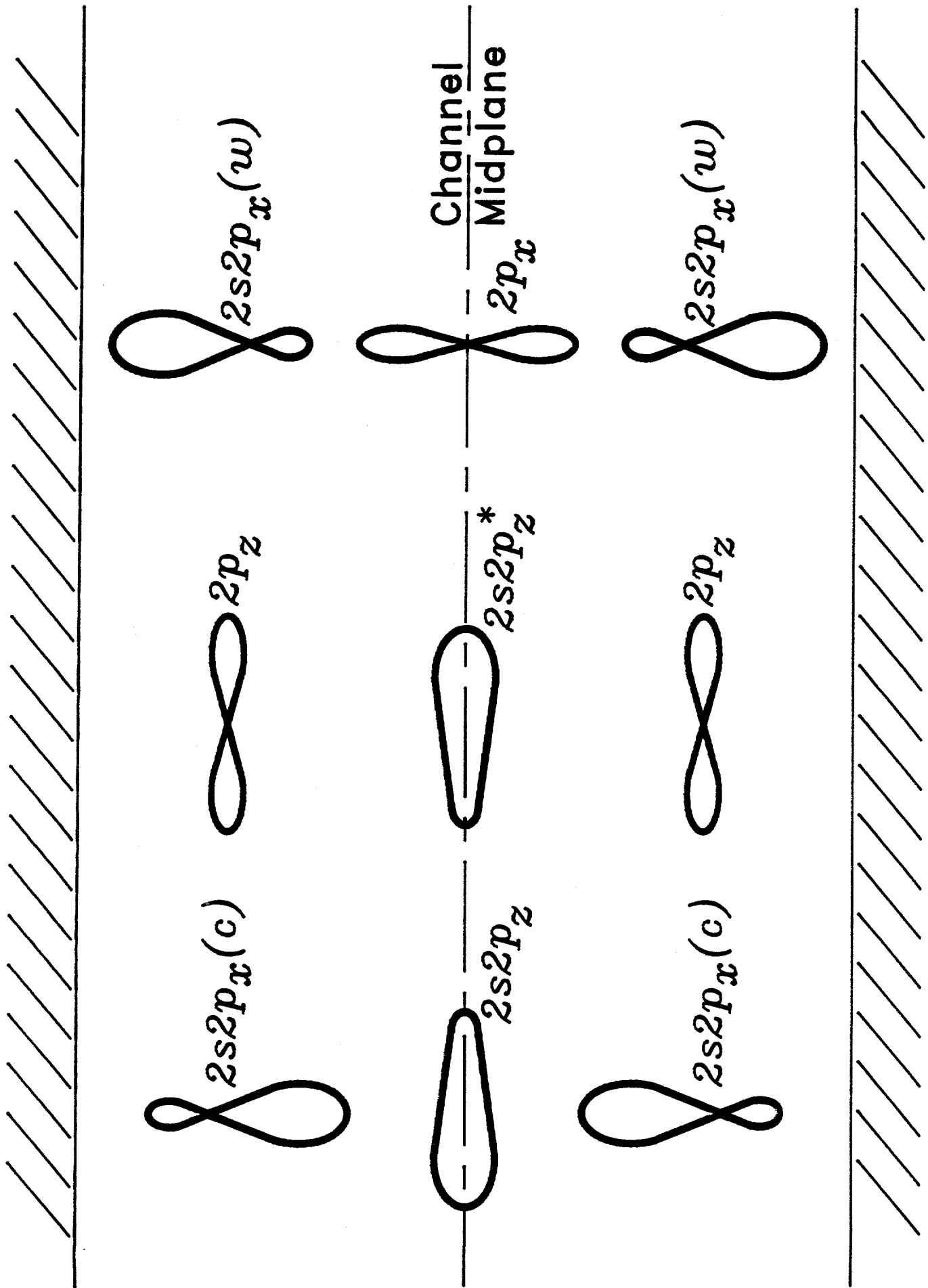


Figure 5

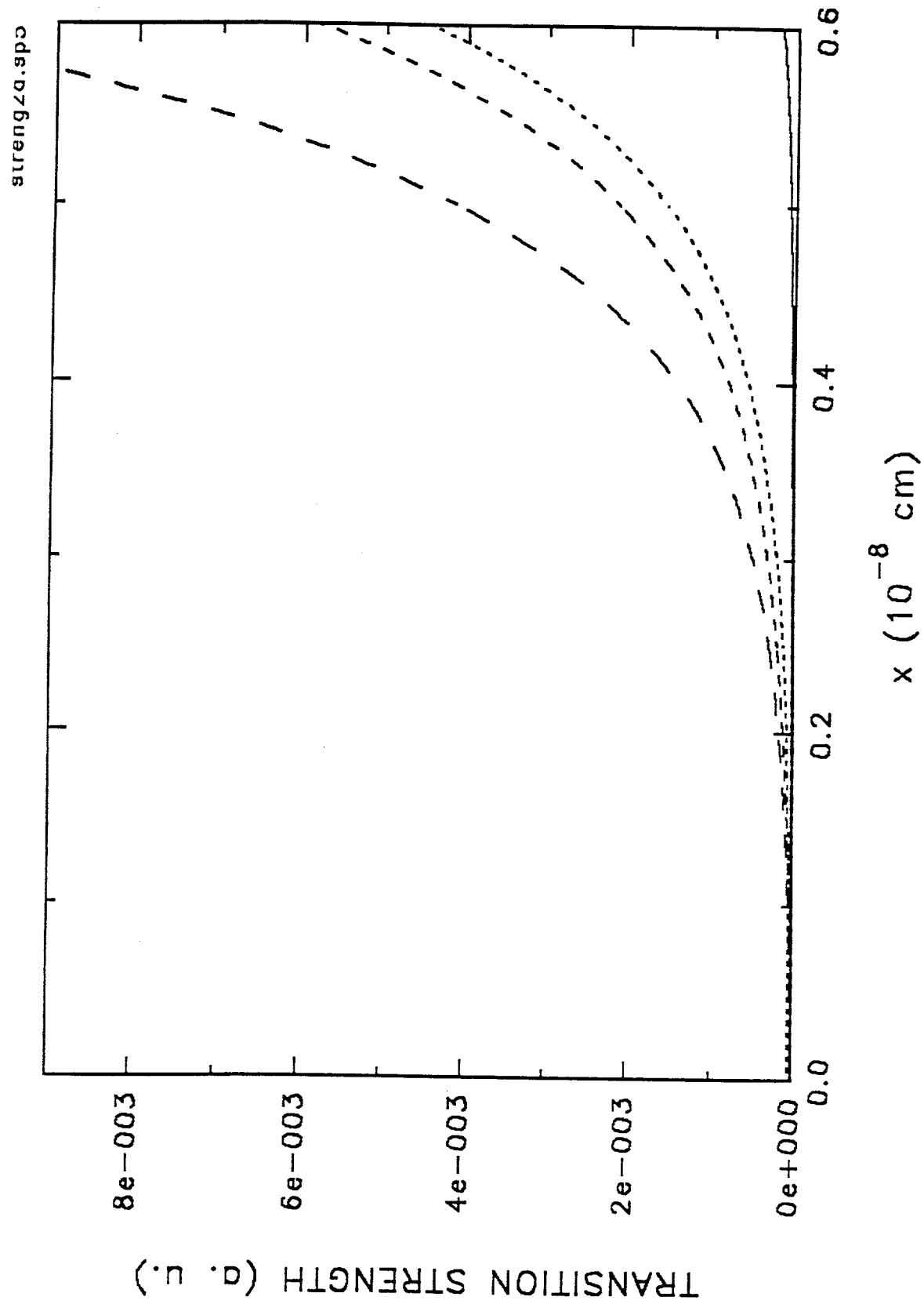


Figure 6

CHANNEL "WALL"

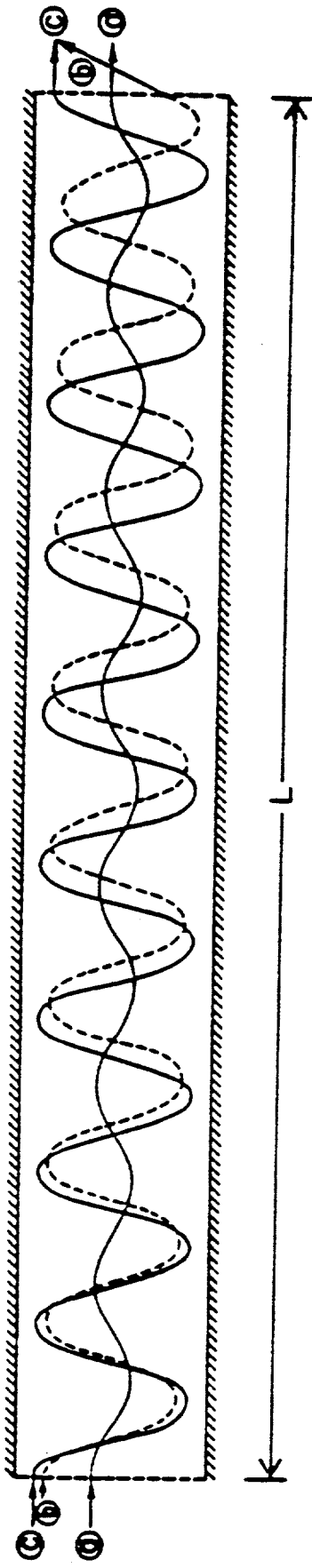


Figure 7

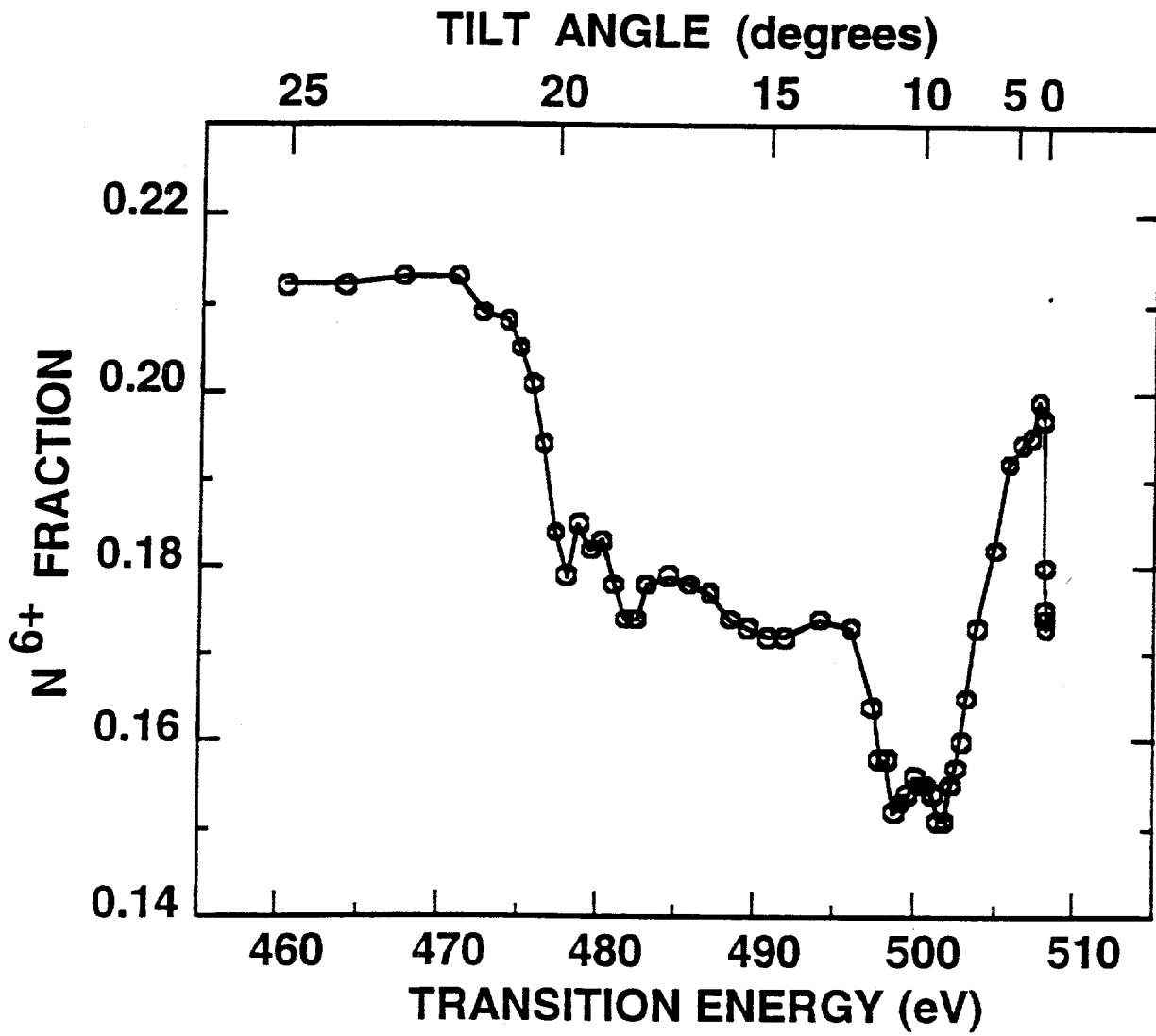


Figure 8

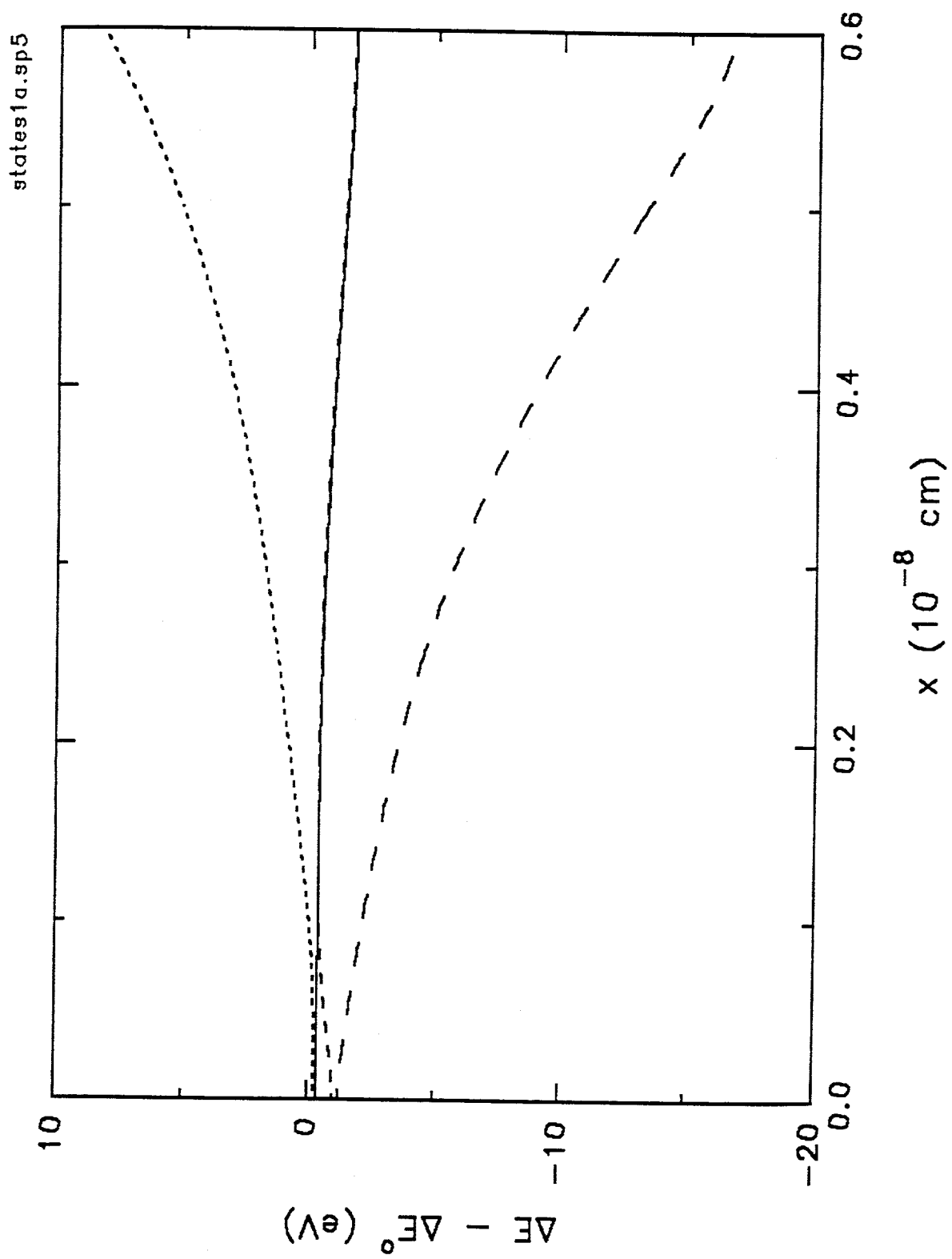


Figure 9

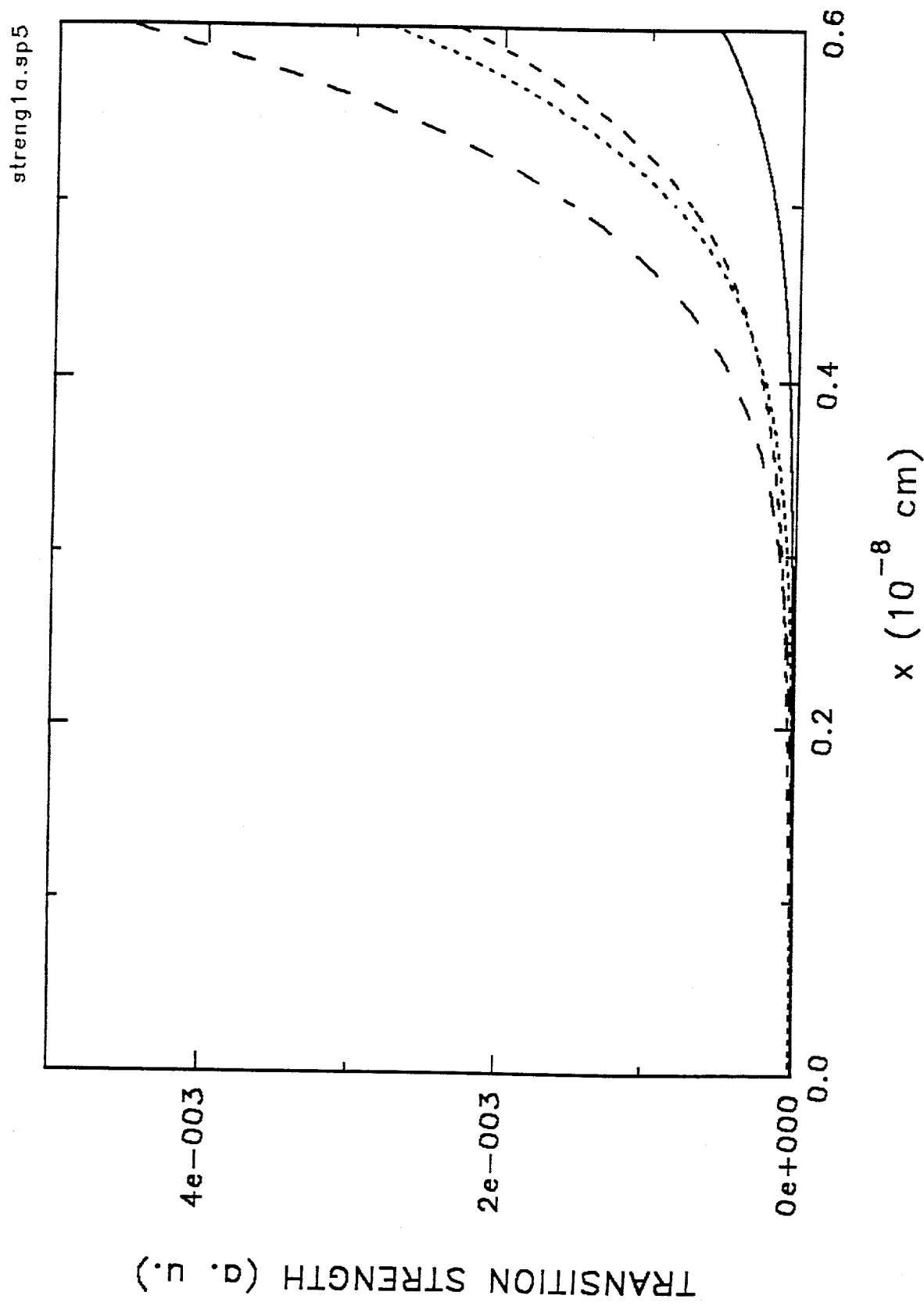


Figure 10

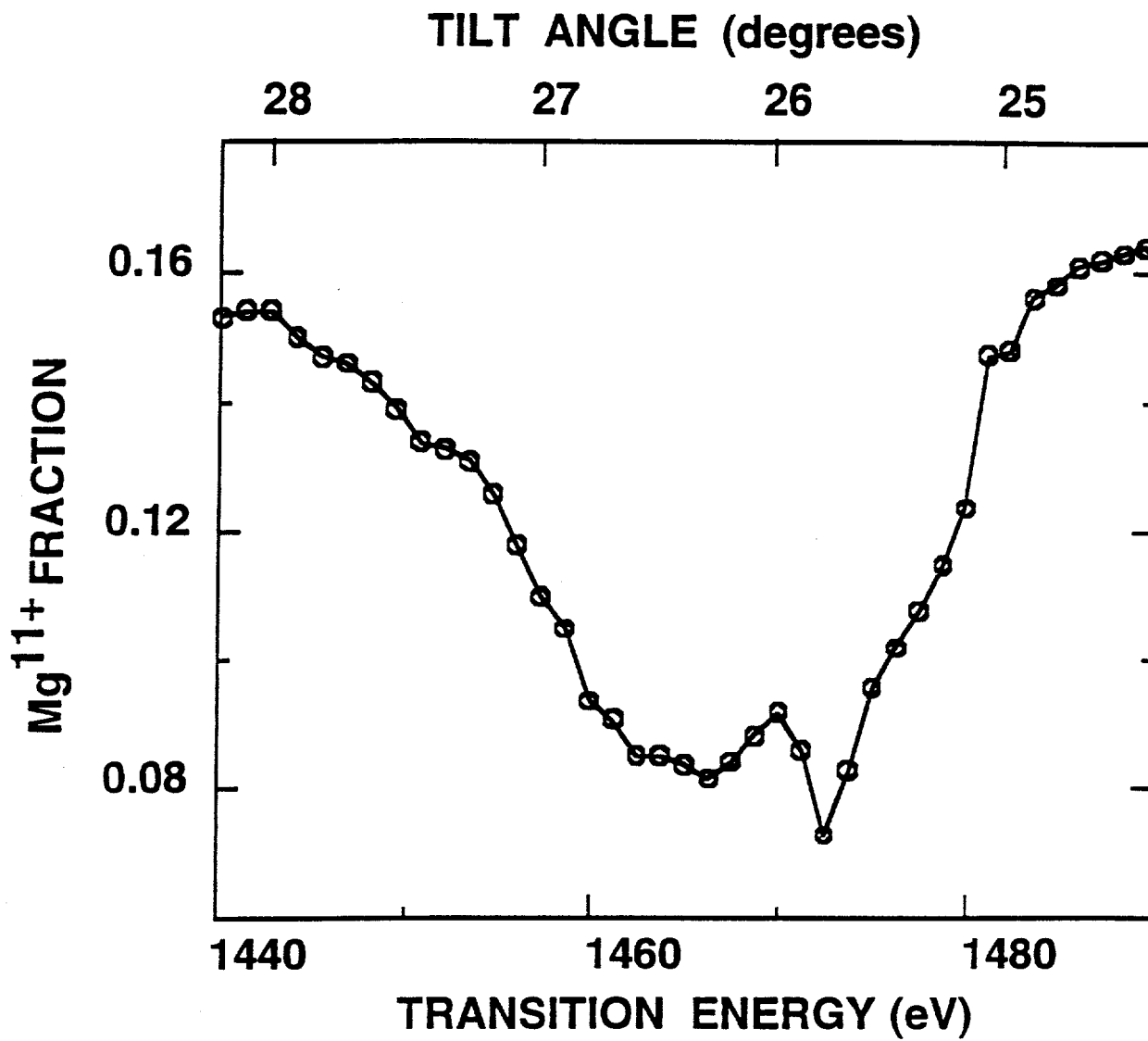


Figure 11

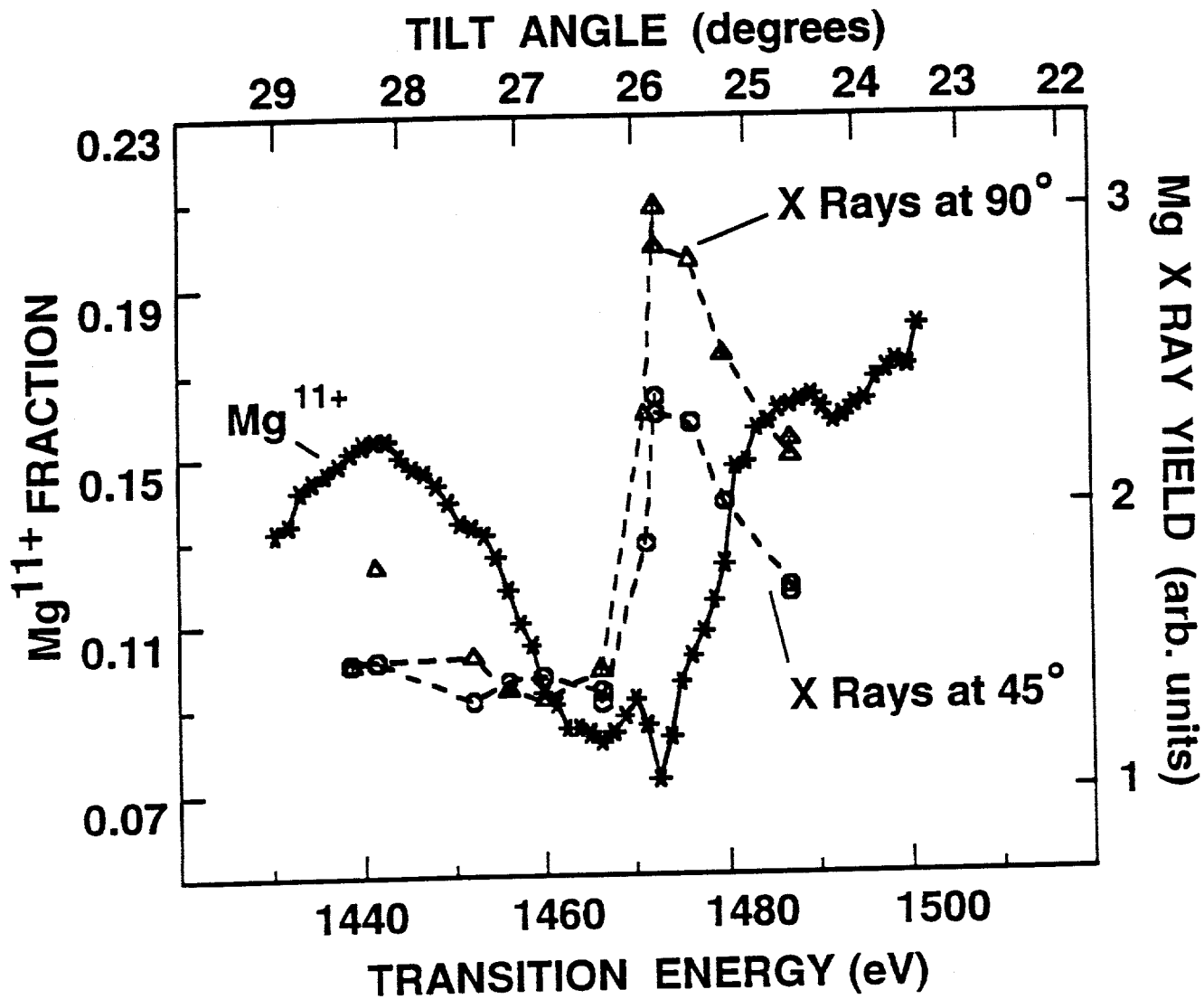


Figure 12